



# Parametric analyses of square reinforced concrete slabs strengthened by fiber-reinforced plastics



Cindrawaty Lesmana, Hsuan-Teh Hu \*

Department of Civil Engineering, National Cheng Kung University, Tainan 701, Taiwan, ROC

## HIGHLIGHTS

- FRP-strengthened RC slabs are investigated by finite element software ABAQUS.
- Proper constitutive models are applied to simulate nonlinear material behavior.
- A proper bond model is found essential to be incorporated into numerical analysis.
- Parametric analyses are performed to examine the behavior of strengthened slabs.

## ARTICLE INFO

### Article history:

Received 30 July 2013

Received in revised form 21 November 2013

Accepted 23 November 2013

### Keywords:

Finite element analysis

Laminates

Slab

## ABSTRACT

The external bonding of fiber-reinforced polymer (FRP) laminates on a tension face is an effective technique for strengthening reinforced concrete (RC) structures. In such application, only a limited amount of research is available on the numerical modeling that includes appropriate constitutive models to simulate the nonlinear material behavior of the structures. The finite element method was used to investigate various effects, from slab thickness, concrete, steel bars and FRP properties to the behaviors and maximum capacities of the FRP-strengthened RC slabs. This paper demonstrates the rationale consideration to design FRP-strengthened RC slabs and the proper modeling of constitutive materials and interfaces essential to simulate suitable behavior of the composites.

© 2013 Elsevier Ltd. All rights reserved.

## 1. Introduction

A significant number of investigations has been conducted on the application of externally bonded fiber-reinforced plastic (FRP) in the strengthening of reinforced concrete (RC) structures [1–3]. Although there has been a considerable amount of research on strengthened beams and columns, applications to RC slabs are in comparison rather limited, especially for strengthened two-way slabs under distributed load. Most research that has been carried out is experimentally based [4,5], and only a limited amount of studies are available on the numerical modeling. The lack of such research creates a challenge for the investigation of numerical modeling using the finite element (FE) method, despite FE being an efficient and cost-effective numerical tool to model the structural behavior of RC members.

Experimental studies are indeed crucial to better understand the failure modes and actual behavior of the structures; however, these types of study are expensive and time consuming and the models are difficult to test until ultimate failure point. To expand FRP utilization and improve the composite design, conducting

numerical studies is essential. FE research on FRP-strengthened RC slabs from the past decade has been reviewed, but only few studies have included nonlinear FE [6,7] and successfully simulated the debonding failure mode [8–10].

Adhesives are commonly used to attach laminates to concrete. This interface is usually considered as a perfect bonding between the FRP and the slab with a ‘no slip’ assumption that has been used by many investigators [3,4,11,12]. However, it is important to include the compliance of the bond between concrete and FRP since most research has been dominated by debonding failure. Bond behavior can be represented as a bond–slip model, such as: the linear–brittle bond–slip model [13] that neglects the softening behavior, an ascending and descending branch of a bond–slip model [14], a precise, simplified, and bilinear bond–slip model [15].

This study was conducted to predict the complete load–deformation behavior up to failure and includes a nonlinear FE analysis for two-way slab strengthening with externally bonded FRP. For accurate FE analysis results, it is essential to adopt an appropriate constitutive material model to define the significant material behavior. Although most research has assumed a linear FRP behavior, unidirectional fibrous composites exhibit severe nonlinearity in regard to their inplane shear stress–strain relations [16]. Deviation from linearity is observed with inplane transverse loading;

\* Corresponding author. Tel.: +886 6 2757575x63168; fax: +886 6 2358542.

E-mail address: [hthu@mail.ncku.edu.tw](mailto:hthu@mail.ncku.edu.tw) (H.-T. Hu).

however, the degree of nonlinearity is not comparable to those observed with inplane shear [17]. Accordingly, this paper introduces the nonlinear behavior, not only for concrete material, but also for FRP material.

A number of factors affect the performance of the bonding mechanism between the FRP and concrete, such as dimensions, mechanical properties and composition of the fibers, as well as the adhesion or bond between the fibers and RC [18]. The linear stress–strain relationship of FRP up to failure without a noticeable yield point creates a sudden failure of the composite. To create a better composite design, it is essential to provide the maximum stiffness with minimum material [18], and to take advantage of the matrix material as the host and FRP material as the embedded anisotropic nature of the material.

The objective of this paper is to investigate the effects of the nonlinear material behavior of composite slabs, including the interface modeling between the RC slab and FRP. Some parametric studies, such as concrete, steel bars and FRP properties, are generated to observe the behavior and the maximum capacity of the composite slabs under specific circumstances. Aspects of the behavior evaluated in this study include the ultimate load of the models, the effects of the parameters on the ultimate load and energy at the failure point, and the effectiveness of the material to improve the design of FRP-strengthened RC slabs. In all simulations, realistic constitutive laws for materials, reasonable interface models, and the reliable verified factors were adopted.

## 2. Nonlinear finite element models

The numerical analysis was carried out using the FE software package ABAQUS [19]. This program can simulate the entire nonlinear load–deformation behavior of conventional and FRP-strengthened RC slabs. The software simulations employ constitutive models for concrete, steel, and FRP. Reliable constitutive models applicable to steel reinforcing bars and concrete are available in the ABAQUS material library; however, the ABAQUS package does not have a nonlinear material library for FRP. Consequently, the resulting nonlinear constitutive equations for the FRP were coded in FORTRAN language as a subroutine and linked to the ABAQUS software. To model the FRP/concrete interface, bond–slip relations were introduced using cohesive behavior that links the FRP laminates to the concrete.

### 2.1. Modeling of concrete

Under multi-axial combinations of loading, the failure strengths of concrete are different from those observed under uni-axial conditions. However, the maximum strength envelope under multiple stress conditions seems to be largely independent of load path [20]. In Fig. 1, a Mohr–Coulomb type compression surface together with a crack detection surface is used to model the failure surface of concrete. When the principal stress components of concrete are in a biaxial compression zone, the response of the concrete is modeled as an elastic–plastic theory with an associated flow and an isotropic hardening rule. When the principal stress components of concrete are in either a biaxial tension zone or in a biaxial tension–compression zone, cracking of concrete is defined to occur by the crack detection surface. Once the cracking of concrete takes place, the orientation of the crack is stored. Damaged elasticity is then used to model the existing crack [19].

When plastic deformation occurs, there should be a specific parameter to guide the expansion of the yield surface. A commonly used approach is to relate the multidimensional stress and strain conditions to a pair of quantities, namely, effective stress  $\sigma_c$  and effective strain  $\epsilon_c$ , such that results obtained following different

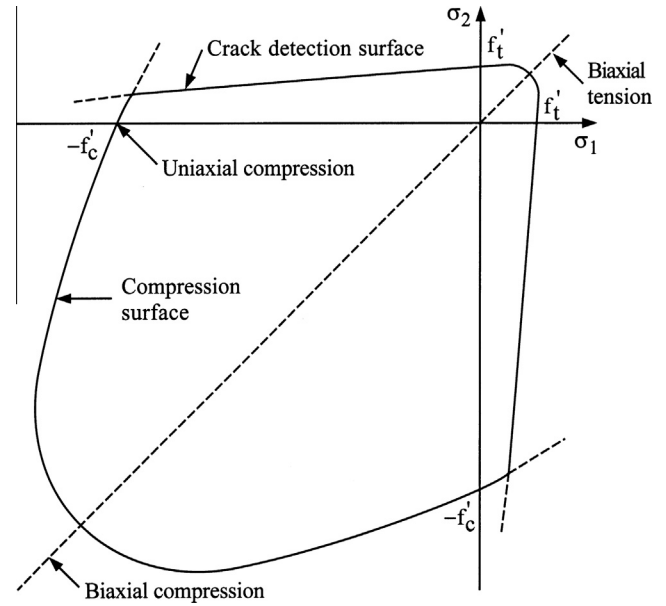


Fig. 1. Concrete failure surface in plane stress.

loading paths can all be correlated by means of the equivalent uni-axial stress–strain curve. For concrete nonlinear behavior, Saenz’s stress–strain curve [21] is used. This relationship has been widely adopted as the uni-axial stress–strain curve for concrete, and has the following form:

$$\sigma_c = \frac{E_c \epsilon_c}{1 + (R + R_E - 2) \left(\frac{\epsilon_c}{\epsilon_o}\right) - (2R - 1) \left(\frac{\epsilon_c}{\epsilon_o}\right)^2 + R \left(\frac{\epsilon_c}{\epsilon_o}\right)^3} \quad (1)$$

where

$$R = \frac{R_E(R_\sigma - 1)}{(R_E - 1)^2} - \frac{1}{R_E}; \quad R_E = \frac{E_c}{E_o}; \quad E_o = \frac{f'_c}{\epsilon_o}$$

and where  $R_\sigma = 4$ , and  $R_E = 4$  are used [22]. In the analysis, Eq. (1) is taken as the equivalent uni-axial stress–strain curve for concrete. The value of  $\epsilon_o$  is 0.003, as suggested by the ACI Committee 318 [23]. The initial modulus of the elasticity of concrete  $E_c$  can be calculated with reasonable accuracy from the empirical equation [23].

When cracking of concrete takes place, a smeared model is used to represent the discontinuous macro crack behavior. Tension stiffening, in which the cracked concrete of the RC element can still carry some tensile stress in the direction normal to the crack [24], is utilized by a simple descending line to model this tension stiffening phenomenon (Fig. 2). The default value of the strain  $\epsilon^*$  at which the tension stiffening stress reduces to zero is 0.001 [19].

During the post cracking stage, the cracked RC can still transfer shear forces through aggregate interlock or shear friction, which is

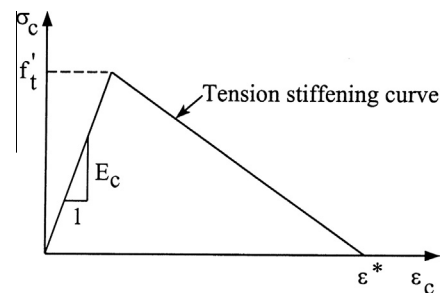


Fig. 2. Tension stiffening model.

termed shear retention. Assuming that the shear modulus of intact concrete is  $G_c$ , then the reduced shear modulus  $\hat{G}$  of cracked concrete can be expressed as  $\hat{G} = \mu G_c$  and  $\mu = (1 - \varepsilon/\varepsilon_{max})$ , where  $\varepsilon$  is the strain normal to the crack direction and  $\varepsilon_{max}$  is the strain at which the parameter  $\mu$  reduces to zero. Numerous analytical results have demonstrated that the particular value chosen for  $\mu$  (between 0 and 1) does not appear to be critical, but that values greater than zero are necessary to prevent numerical instabilities [24,25]. In ABAQUS,  $\varepsilon_{max}$  is usually assumed to be a very large value, i.e.,  $\mu = 1$  (full shear retention). As such, in this investigation, the default values for the tension stiffening parameter  $\varepsilon^* = 0.001$  and shear retention parameter  $\mu = 1$  are used.

2.2. Modeling of steel and FRP reinforcement

The perfectly elastic plastic is assumed to exemplify the stress-strain curve of the reinforcing bar, which the elastic modulus of the steel reinforcement ( $E_s$ ) is 200 GPa. Although a bond-slip relation is assumed for the FRP/concrete interface, the concrete and steel reinforcement are assumed to be perfectly bonding.

For FRP, each lamina can be considered to be an orthotropic layer in a plane stress condition. It is well known that unidirectional fibrous composites exhibit severe nonlinearity in their in-plane shear stress-strain relation. To model this shear behavior, the nonlinear strain-stress relation for a composite lamina suggested by Hahn and Tsai [16] is adopted as follows:

$$\begin{Bmatrix} \varepsilon_1 \\ \varepsilon_2 \\ \gamma_{12} \end{Bmatrix} = \begin{bmatrix} \frac{1}{E_{11}} & -\frac{\nu_{21}}{E_{22}} & 0 \\ -\frac{\nu_{12}}{E_{11}} & \frac{1}{E_{22}} & 0 \\ 0 & 0 & \frac{1}{G_{12}} \end{bmatrix} \begin{Bmatrix} \sigma_1 \\ \sigma_2 \\ \tau_{12} \end{Bmatrix} + S_{6666} \tau_{12}^2 \begin{Bmatrix} 0 \\ 0 \\ \tau_{12} \end{Bmatrix} \quad (2)$$

In this model, only one constant  $S_{6666}$  is required to account for the inplane shear nonlinearity, the value of which can be determined by a curve fit to various off-axis tension test data [16].

The incremental stress-strain relations for a nonlinear orthotropic lamina can be given as follows:

$$\Delta\{\sigma'\} = [Q'_1]\Delta\{\varepsilon'\} \quad (3)$$

$$\Delta\{\tau'_i\} = [Q'_2]\Delta\{\gamma'_i\} \quad (4)$$

where  $\Delta\{\sigma'\} = \Delta\{\sigma_1, \sigma_2, \tau_{12}\}^T$ ;  $\Delta\{\tau'_i\} = \Delta\{\tau_{13}, \tau_{22}\}^T$ ;  $\Delta\{\varepsilon'\} = \Delta\{\varepsilon_1, \varepsilon_2, \gamma_{12}\}^T$ ;  $\Delta\{\gamma'_i\} = \Delta\{\gamma_{13}, \gamma_{22}\}^T$ ;

$$[Q'_1] = \begin{bmatrix} \frac{E_{11}}{1-\nu_{12}\nu_{21}} & \frac{\nu_{12}E_{22}}{1-\nu_{12}\nu_{21}} & 0 \\ \frac{\nu_{21}E_{11}}{1-\nu_{12}\nu_{21}} & \frac{E_{22}}{1-\nu_{12}\nu_{21}} & 0 \\ 0 & 0 & \frac{1}{\frac{1}{G_{12}} - 3S_{6666}\tau_{12}^2} \end{bmatrix} \quad (5)$$

$$[Q'_2] = \begin{bmatrix} \alpha_1 G_{13} & 0 \\ 0 & \alpha_2 G_{23} \end{bmatrix} \quad (6)$$

The terms  $\alpha_1$  and  $\alpha_2$  are the shear correction factors, and are taken to be 0.83 [26]. Furthermore, it is assumed that the transverse shear stresses always behave linearly and do not affect the nonlinear behavior of any inplane shear.

Among existing failure criteria, the Tsai-Wu criterion [27] has been extensively used in the literature and is adopted in this analysis. Under plane stress conditions, this failure criterion has the following form:

$$F_1\sigma_1 + F_2\sigma_2 + F_{11}\sigma_1^2 + 2F_{12}\sigma_1\sigma_2 + F_{22}\sigma_2^2 + F_{66}\tau_{12}^2 = 1 \quad (7)$$

with

$$F_1 = \frac{1}{\bar{X}} + \frac{1}{\bar{X}'}, F_2 = \frac{1}{\bar{Y}} + \frac{1}{\bar{Y}'}, F_{11} = \frac{-1}{\bar{X}\bar{X}'}, F_{22} = \frac{-1}{\bar{Y}\bar{Y}'}, F_{66} = \frac{1}{\bar{S}^2}$$

$\bar{X}$ ,  $\bar{Y}$  and  $\bar{X}'$ ,  $\bar{Y}'$  are the lamina longitudinal and transverse strengths in tension and compression, respectively, while  $\bar{S}$  is the shear strength of the lamina. Although it is difficult to determine the stress interaction term  $F_{12}$  in Eq. (7), it has been suggested that  $F_{12}$  can be set equal to zero for practical engineering applications [28]. Therefore,  $F_{12} = 0$  is used in this investigation.

2.3. FRP/concrete interface

Two models are presented in this paper, fully bonded behavior and cohesive behavior. For the fully bonded behavior, the contribution of the adhesive layer to the flexural capacity was neglected. For the cohesive behavior, the interface between concrete and FRP is integrated to the model to simulate the bond behavior of the composite. Bond properties modeled as inputs to the cohesive model, such as initial stiffness related to adhesive properties, shear strength and fracture energy, are expressed as functions of the tensile strength of concrete and of adhesive properties.

The mechanical behavior of the FRP/concrete interface is modeled as a relationship between the local stress and the relative displacement. The properties of the interface elements were determined from the simplified bilinear bond-slip model [15] illustrated in Fig. 3. A damage evolution law was defined such that the bond-slip curve unloads linearly through the origin after the interface enters the softening range. The maximum bond/shear stress experienced by the interface,  $\tau_{max}$ , and corresponding slip when the bond stress reaches maximum,  $S_o$ , are governed by the tensile strength of the concrete and a width ratio parameter,  $\beta_w$ . The maximum local bond strength  $\tau_{max}$  and the corresponding slip  $S_o$  are given by

$$\tau_{max} = 1.5\beta_w f_t \quad (8)$$

$$S_o = 0.0195\beta_w f_t \quad (9)$$

The parameter  $\beta_w$  is defined in terms of the laminate width,  $w_f$ , the spacing,  $s_f$ , and angle of fiber orientation to longitudinal axis,  $\beta$  [9], as follows

$$\beta_w = \sqrt{\frac{2 - w_f/(s_f \sin \beta)}{1 + w_f/(s_f \sin \beta)}} \quad (10)$$

The initial stiffness [10] of the bond-slip model is defined by

$$K_o = \frac{K_a K_c}{(K_a + K_c)} \quad (11)$$

where  $K_a = G_a/t_a$  and  $K_c = G_c/t_c$ .  $G_a$  is the elastic shear modulus of the adhesive and  $t_a$  is the effective thickness of the adhesive.  $G_c$  is the elastic shear modulus of the concrete and  $t_c$  is the effective thickness of the concrete whose deformation forms part of the interfacial slip.

The total fracture energy can be expressed as:

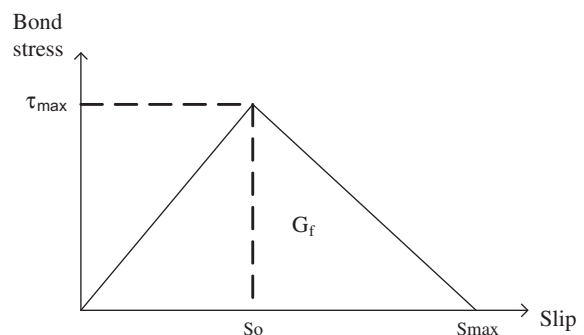


Fig. 3. Bond-slip models.

$$G_f = 0.308\beta_w^2\sqrt{f_t} \quad (12)$$

Although the interfacial fracture energy is less affected by the FRP stiffness, it is affected by the mechanical properties of the concrete and to a lesser extent by those of the adhesive [10].

### 3. Geometrical modeling

The slab's models were adopted from the experimental investigation by Mosallam and Mosalam [4]. The slabs were subjected to uniform static pressure with dimension, as in Fig. 4. Pressure was applied to the bottom surface of the slab so that the top surface was subjected to tensile stress. An equal spacing in the two orthogonal directions #3 @ 305 mm was used for tension reinforcement with grade 60. The yielding stress was  $f_y = 413.7$  MPa, and the compressive strength of the concrete was  $f'_c = 32.87$  MPa.

Due to geometrical and loading symmetry, only a quarter of the simply supported slab in Fig. 4 was analyzed, with symmetric boundary conditions assigned along two symmetric planes. The finite element mesh has 25 reinforced concrete shell elements with 9 layers through the thickness in total (5 rows in each FRP strip direction). RC rectangular slabs and FRP were modeled by four-node quadrilateral shell elements with six degrees of freedom per node. The rebar/concrete interface, such as the bond slip and dowel action, are modeled approximately by introducing some "tension stiffening" into the concrete cracking model to simulate load transfer across cracks through the rebar. An incremental-iterative Newton's method was applied to solve the nonlinear equilibrium equations.

While one specimen was a pure RC slab, the other specimen was an RC slab strengthened with two FRP layers, of which their fiber directions were oriented in the two orthogonal directions of the slab (Fig. 4). The thickness for each layer is 0.58 mm adhered to the top side of the slab. At the intersection regions of the staggered unidirectional laminates, bidirectional fiber architecture, i.e. a [90/0/90/0] lamination layup, was formed. The material properties of carbon FRP were adopted from the experimental

specimens of Mosallam and Mosalam [4]. The tensile strength ( $X_{ut}$ ) was 1208.7 MPa while elastic modulus ( $E_{11}$ ) was 100.75 GPa. The following parameters were assumed to take the Tsai–Wu criterion into account:  $E_{22} = 1$  GPa,  $G_{12} = 1$  GPa,  $X_{uc} = -12$  MPa,  $Y_{uc} = 12$  MPa,  $Y_{ut} = -12$  MPa, and  $\nu_{12} = 0.3$ .

### 4. Parametric studies

In the following, comparisons are made between the experimental and numerical results in terms of the ultimate load carrying capacities and load–displacement relationships. The simulated specimens include control and FRP-strengthened RC slabs. The FE constitutive models for steel bars, FRP and RC were validated against the test results reported in the literature [6,19]. The parametric studies are organized on four important factors: composite slabs, dimension, concrete, steel bars, and FRP. Three thickness variants are represented by dimension ratios ( $L/h$ ) which is the ratio between the length and thickness of the slabs. The ratios are 20, 35, and 40 for the slab thicknesses of 132 mm, 76 mm, and 66 mm, respectively. The ratio 35 with thickness 76 mm is the reference slab from Mosallam–Mosalam. The concrete strength properties are 25 MPa, 32.87 MPa, and 40 MPa. The influence of the steel bars are measured by steel reinforcement ratios ( $\rho_s = 0.18\%$ ,  $\rho_s = 0.37\%$ , and  $\rho_s = 1\%$ ) and steel strength (grade 40 –  $f_y = 276$  MPa and grade 60 –  $f_y = 413.7$  MPa). It should be noticed that concrete strength property 32.87 MPa and  $\rho_s = 0.37\%$  with grade 60 is the reference slab from Mosallam–Mosalam. The strengthening schemes are categorized into two types: type 1 – the same FRP model as Mosallam and Mosallam's experiments; and, type 2 – a cross formed by two strips of FRP removed in both directions from the existing models. The number of layers and different FRP properties were also investigated. Details of all variations for the parametric studies are summarized in Table 1.

#### 4.1. Verification of the proposed model

A comparison between the FE predictions and the experimental results, with and without FRP, are presented to demonstrate the capability of the present FE model in simulating the failure of the structures. Fig. 5 presents verification of simulation models that compare FE results with the test results. The FE results for load–displacement at the center can simulate real behavior up to failure of the control and FRP-strengthened models. The predicted ultimate load and displacement for the RC slab are very close to the test results with error percentages of 3.4% and 2.1%, respectively. For the FRP-strengthened RC slabs, two assumptions were adopted: fully bonded (FB) and cohesive behavior (CB). The FE results for FB can predict the load well (0.01% error); however, if compared to CB (1.3% error), the FB curve only has significant results in the early section of the curve. As the steel yields, the FB curve becomes stiffer, so the error percentages of the final displacement of the experimental models are 16.6% (FB) and 5.9% (CB). Although both assumptions are good for predicting ultimate load, to obtain accurate FE results for load–deformation behavior, the cohesive assumption is recommended. In further parametric studies (Table 1), the FE results are based on the cohesive model assumptions.

Fig. 6 shows the effects of the tension stiffening are not significant to the ultimate load. The factor of tension stiffening is based on bond slip between the reinforcement and the surrounding concrete. From the figure, it can be observed that the effects of tension stiffening are only in the early stage of the load–displacement curves. Since this study only consider the maximum total load, so that the default value of 0.001 in ABAQUS is used.

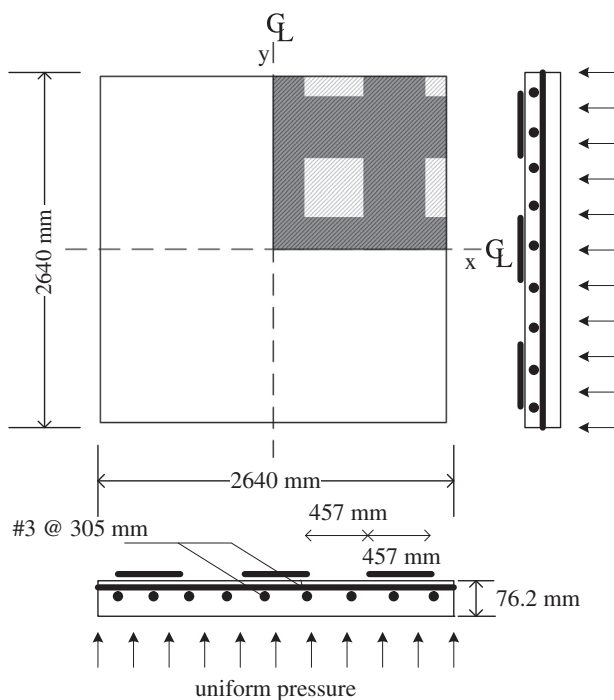
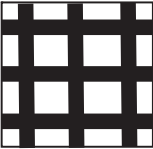
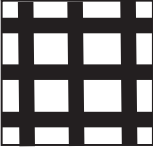
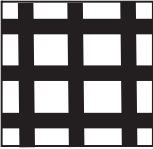
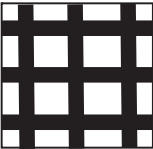
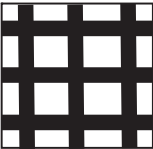
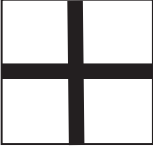


Fig. 4. Details of Mosallam–Mosalam's specimens.

**Table 1**  
Dimension and property variations in parametric studies.

Models	Dimension $L/h$	Concrete $f'_c$ (MPa)	Steel		FRP		Material properties	Type
			$\rho_s$ (%)	$f_{ys}$ (MPa)	No. of layers			
1	20, 40	33	0.37	414	2		$X_{ut} = 1209$ MPa $E_{11} = 101$ GPa	1 
2	20, 40	25, 40	0.37	414	2		$X_{ut} = 1209$ MPa $E_{11} = 101$ GPa	1 
3	35	33	0.18, 0.37, 1	276	2		$X_{ut} = 1209$ MPa $E_{11} = 101$ GPa	1 
4	35	33	0.37	414	1, 3, 4		$X_{ut} = 1209$ MPa $E_{11} = 101$ GPa	1 
5	35	33	0.37	414	2		$X_{ut} = 2400$ MPa $E_{11} = 155$ GPa	1 
6	35	33	0.37	414	2		$X_{ut} = 1209$ MPa $E_{11} = 101$ GPa	2 

#### 4.2. Ultimate load analysis of the slabs with thickness variations

The load displacement curves shown in Fig. 7 are specified for  $f'_c = 32.87$  MPa,  $\rho_s = 0.37\%$  with grade 60, type 1 strengthening with 2 layers FRP laminates in ply combinations [90/0] for  $X_{ut} = 1209$  MPa, and three different dimension ratios ( $L/h = 20, 35,$  and  $40$ ). Taking the  $L/h = 35$  case as a base point (the Mosallam–Mosalam's slab), the ultimate load is decreased 26% for RC slabs and 12% for FRP-strengthened RC slabs (SS), if the thickness is decreased 13% ( $L/h = 40$  case); however, if the thickness is increased 74% ( $L/h = 20$  case), the ultimate load can be increased up to 2.5 and 2.3 times for RC and SS, respectively. The behaviors of both RC and SS slabs are similar, and as the dimension ratios become lower, the thickness and ultimate load become higher. The greater the thickness of the slab, the more energy it can absorb. The strengths of pure RC and the composite are affected by the thickness of the

slabs. However, as the thickness decreases, the effects of FRP as a strengthening material are more significant.

For most of cases in Fig. 7 (RC), the first yielding of the steel bars (YS) that defined as the point at which the strain of the rebar reaches  $\epsilon_y$  are occurred first, then followed by the failure of concrete, termed concrete crushing (CC), that assumed for the strain of the concrete becomes greater than 0.003. However, the failure modes of all cases in SS occur when the steel yielding is followed by intact FRP and concrete crushing. The first yielding of the FRP (YF) is when the FRP strain of one or more elements has already reached 0.0023.

Furthermore, the strain energy of the models is observed. The energy stored at failure (U) is defined as the total area under the load and displacement curves. The energy results of the RC models for  $L/h = 20, 35,$  and  $40$  are 12.6 kNm, 11.5 kNm, and 7.9 kNm, respectively. Similar trends can be found for the energy results of

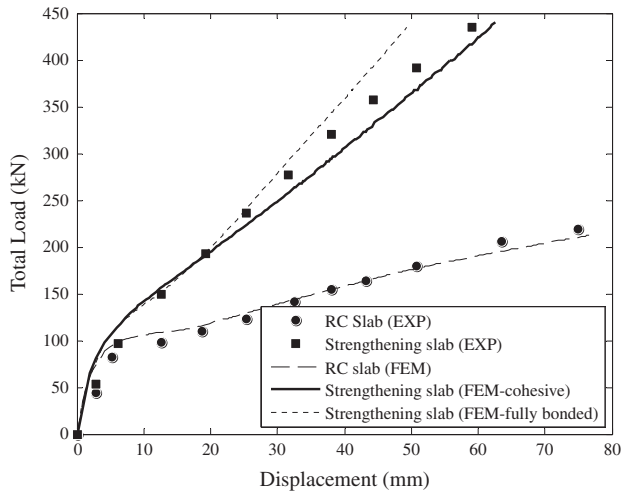


Fig. 5. Load and mid-span displacement behaviors of RC square slabs with and without FRP.

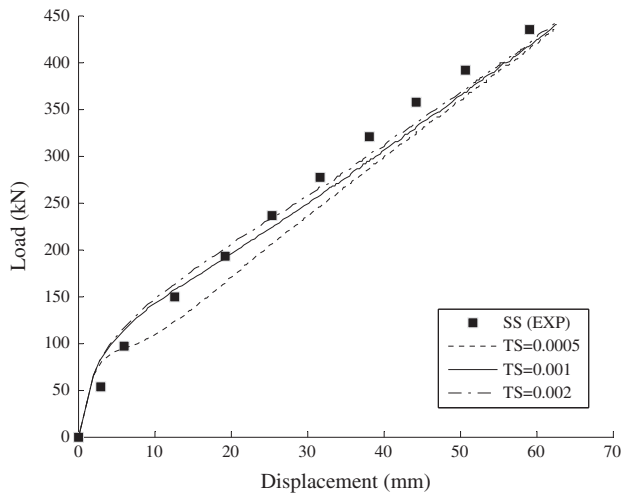


Fig. 6. Load and mid-span displacement behaviors of RC square slabs with FRP in various tension stiffening.

the SS models for  $L/h = 20, 35,$  and  $40$  (25 kNm, 16 kNm, and 15 kNm, respectively). Compared to  $L/h = 20$ , a decrease in the thickness of about 42% can lower  $U$  up to 9% (RC) and 36% (SS), while a decrease in the thickness by half can lower  $U$  up to 37% (RC) and 40% (SS). Decreasing the thickness is the same as having a higher  $L/h$  value. By contrast, the lower dimension ratios generate higher strain energy, which affects  $U$  of RC more than the SS model in some levels. These results show that FRP is indeed able to strengthen the RC slabs since it can cover the lack of concrete capacity due to small thickness.

#### 4.3. Ultimate load analysis of the slabs with variation of concrete properties

Fig. 8 presents the load displacement curves for three variations of  $f'_c$  (25, 33, and 40 MPa),  $L/h = 35$ ,  $\rho_s = 0.37\%$  with grade 60, and type 1 strengthening with 2 layers of FRP laminates for  $X_{ut} = 1209$  MPa. Since the curves seem parallel, this demonstrates that the concrete properties have little influence on the behavior of the slabs for RC both without and with FRP. Two layers of adhered FRP in various concrete properties can increase the ultimate load to approximately two times the original load. Compared to

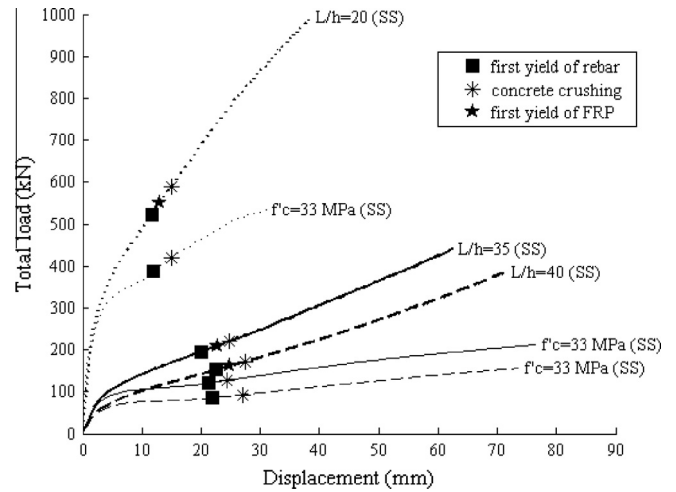


Fig. 7. Load and mid-span behaviors of RC square slabs with and without FRP for variation of thicknesses ( $L = 2640$  mm).

$f'_c = 25$  MPa, if the compression strength of the concrete increases to 7.9 MPa, the ultimate loads are increased 3% (RC) and 14% (SS), but if  $f'_c$  increases to 15 MPa, the ultimate loads are increased 4% (RC) and 29% (SS). The effects of  $f'_c$  are more significant in SS slabs, where doubling the increase of  $f'_c$  can double the increase of the ultimate load.

For all cases of failure modes in Fig. 8 both RC and SS slabs, the first yield of steel always comes first and the last mode is concrete crushing. So that in SS slabs, the first yield of FRP is the mode in between of first yield of steel and concrete crushing.

The results of energy stored at failure for  $f'_c = 25, 33,$  and  $40$  MPa are 13, 16, and 19, respectively. The strain energy is increased as the value of the concrete strength becomes higher. A “tough” composite is the FRP-strengthened RC slab that has a high energy value with minimum material. For this case, the effectiveness of the composite to dimension and concrete properties is measured by the ratio between the strain energy and parameter index. This index is calculated as the multiplication area of the concrete section ( $L \times h$ ) with  $f'_c$ . Fig. 9 shows that the dimension ratio affects the effectiveness of the composite rather than concrete strength, since the difference among  $L/h$  curves is bigger than the difference among  $f'_c$ . The best case is the slab with a higher effectiveness

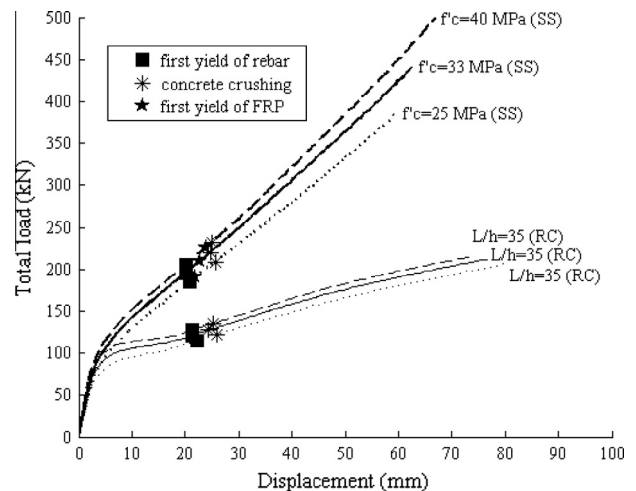


Fig. 8. Load and mid-span behaviors of RC square slabs with and without FRP for variations of concrete properties.

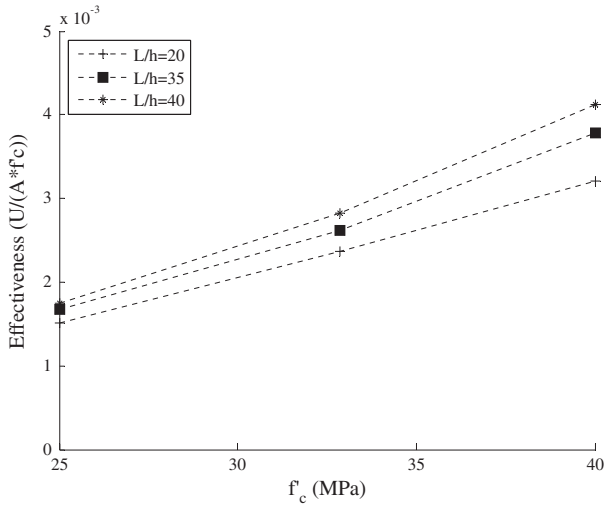


Fig. 9. Effectiveness of FRP-strengthened RC slabs to concrete properties and dimension ratios.

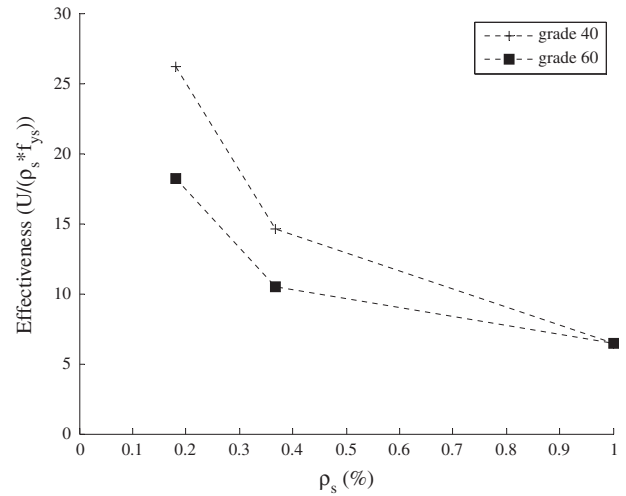


Fig. 12. Effectiveness of FRP-strengthened RC slabs to steel properties.

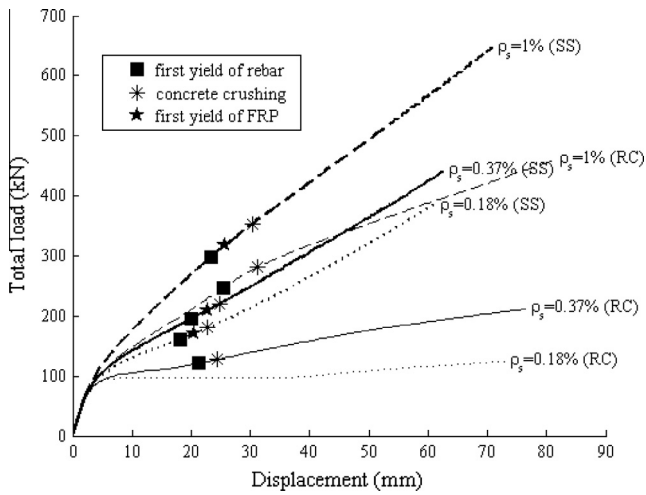


Fig. 10. Load and mid-span behaviors of RC square slabs with and without FRP for variations of steel reinforcement.

value, which is the slab with the higher  $f'_c$  and higher  $L/h$  equaling a lower thickness value.

#### 4.4. Ultimate analysis of RC slabs with variation of steel bars

The higher the value of steel reinforcement ratio, the higher the obtainable ultimate load can be achieved. Fig. 10 illustrates that the ultimate load will significantly increase in tandem with an increasing steel reinforcement ratio for three variations of steel properties grade 60 with  $L/h = 35$ ,  $f'_c = 32.87$  MPa, and type 1 strengthening with 2 layers of FRP laminates for  $X_{ut} = 1209$  MPa. As examples, the ultimate loads for the case  $\rho_s = 0.18\%$ , are 124 kN (RC) and 376 kN (SS), which are smaller than the ultimate loads for the case with  $\rho_s = 1\%$ , 459 kN (RC) and 636 kN (SS). Adding more steel in the slabs enables a higher ultimate load; consequently the curves become more linear as the ratios become higher. In comparing the ultimate loads between SS and RC, the ultimate loads of the composite are 3.1 times greater for the  $\rho_s = 0.18\%$  case, 2.1 times for the  $\rho_s = 0.37\%$  case, and 1.4 times for the case  $\rho_s = 1\%$  case. As the ratios increase, the curves of the slabs with and without FRP become coincident. The increased  $\rho_s$  is not very efficient for the SS models.

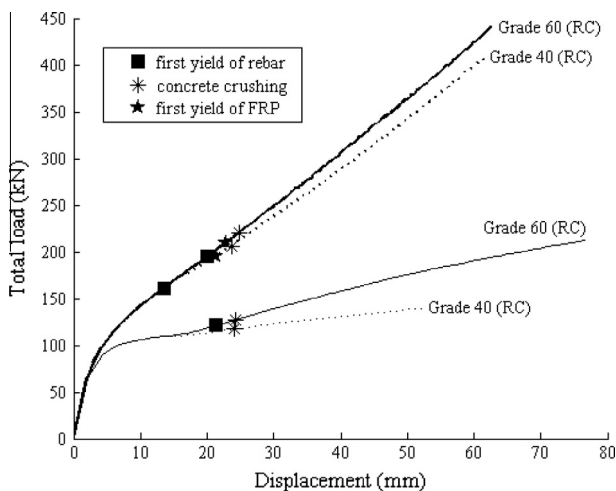


Fig. 11. Load and mid-span behaviors of RC square slabs with and without FRP for variations of steel strength.

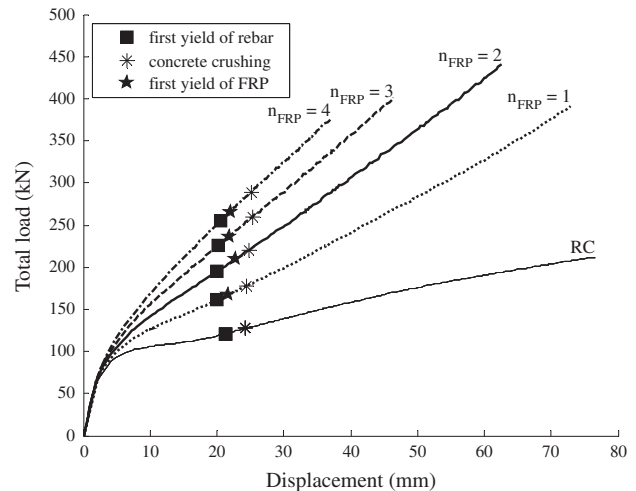


Fig. 13. Load and mid-span behaviors of FRP-strengthened RC slabs for different numbers of FRP layers.

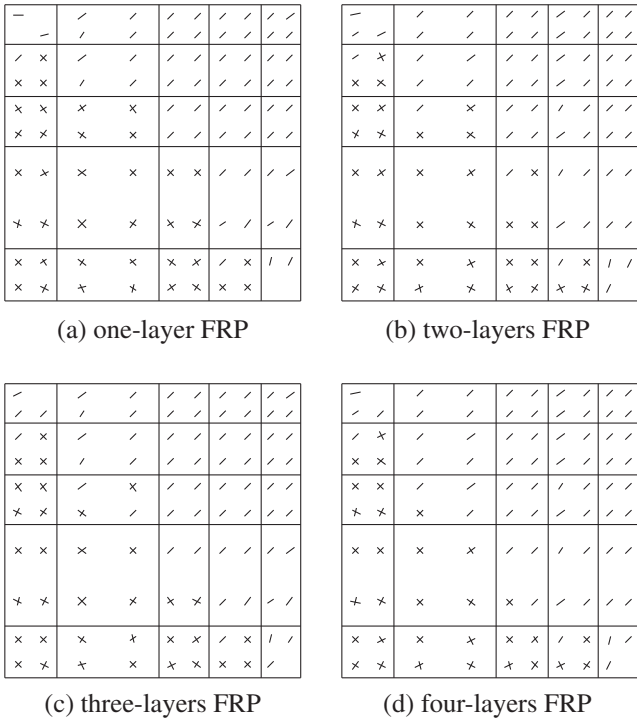


Fig. 14. Crack patterns at failure point for FRP-strengthened RC slabs.

Fig. 11 offers a comparison of the load displacement curves for different steel strengths with  $f'_c = 32.87$  MPa,  $L/h = 35$ ,  $\rho_s = 0.37\%$ , and type 1 strengthening with 2 layers of FRP laminates for  $X_{ut} = 1209$  MPa. The variation of steel strength accounts for only a small effect on the strengthened slab, 8% for the ultimate load and 2% for the maximum displacement; however, a significant effect can be found on pure RC, results of which are 52% for the ultimate

load and 47% for the maximum displacement. FRP adhered onto RC slabs can increase the ultimate load up to 2.9 times for grade 40 and 2.1 times for grade 60. The increased steel strength is superior for RC compared to SS, but using lower steel strength is recommended for utilizing FRP in SS slabs since it can obtain similar result as higher steel strength. These significant results demonstrate that FRP can replace a lack of steel in some cases. Similar to other cases, the Figs. 10 and 11 show that the first yield of steel bar occurs first and the last is concrete crushing. For the SS slabs, the first yield of FRP occurs in between YF and CC.

The results for strain energy of the SS in grade 60 are 13, 16, and 27 for  $\rho_s = 0.18\%$ ,  $\rho_s = 0.37\%$ , and  $\rho_s = 1\%$ , respectively, while the strain energy of the SS slabs for  $\rho_s = 0.37\%$  grade 40 is 15. The small difference in the strain energy results for the effects of the steel strength shows that the strain energy is more affected by steel reinforcement ratios than steel strength. Fig. 12 presents the effectiveness of the composite to rebar properties ( $\rho_s * f_{ys}$ ). A higher value of effectiveness represents a better performance of the composite slabs in creating higher strain energy with minimum material. The effects of steel strength are more significant in obtaining “tough” composites for lower steel properties. As the properties of steel bars and the steel strength become lower, the effectiveness becomes higher.

4.5. Ultimate load analysis of RC slabs with variations of FRP reinforcement

The first yielding of the steel bars (YS) is defined as the point at which the strain of the rebar reaches 0.0021, while the first yielding of the FRP (YF) is when the FRP strain of one or more elements have already reached 0.0023. The failure of concrete, termed concrete crushing (CC), is assumed when the strain of the concrete becomes greater than 0.003. The failure modes of all cases (Fig. 13) occur when the steel yielding is followed by concrete crushing and intact FRP.

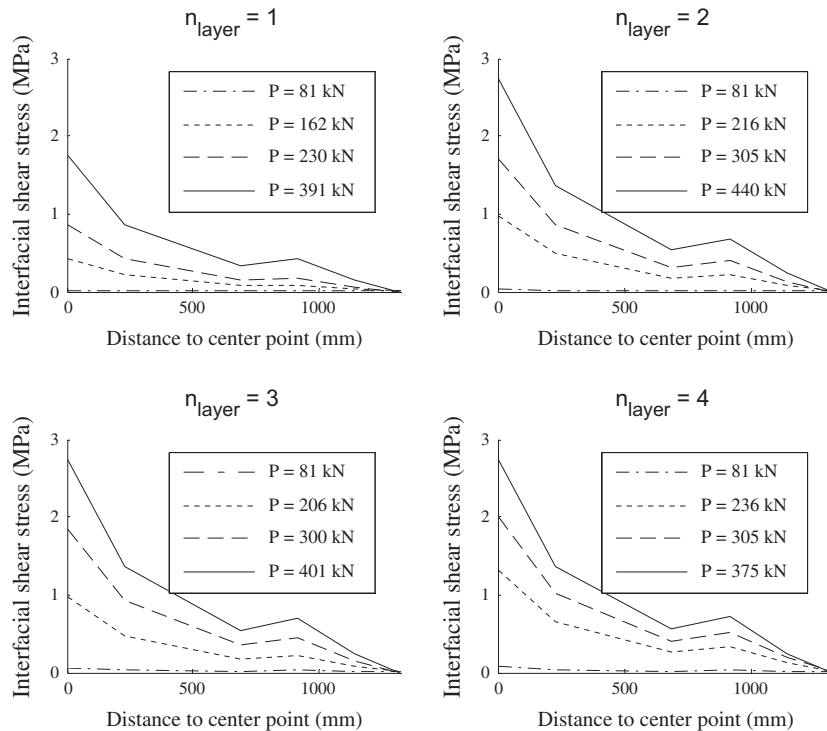
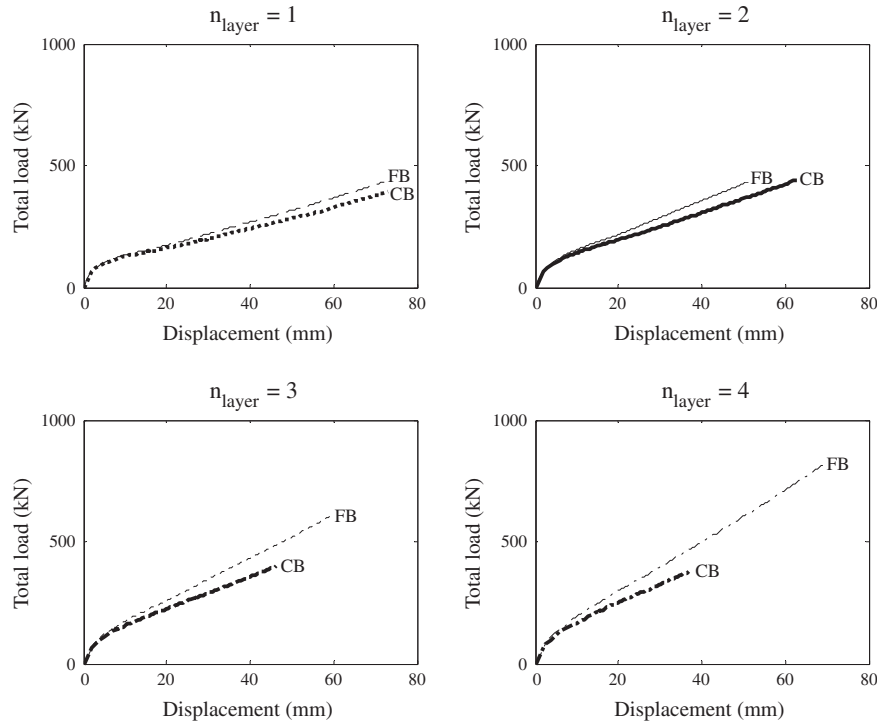


Fig. 15. Interfacial shear stress of FRP-strengthened RC slabs for different numbers of FRP layers cases.





**Fig. 16.** Load and mid-span displacement behaviors of FRP-strengthened RC slabs for different numbers of FRP layers using both the fully bonded (FB) and cohesive behavior (CB) assumption.

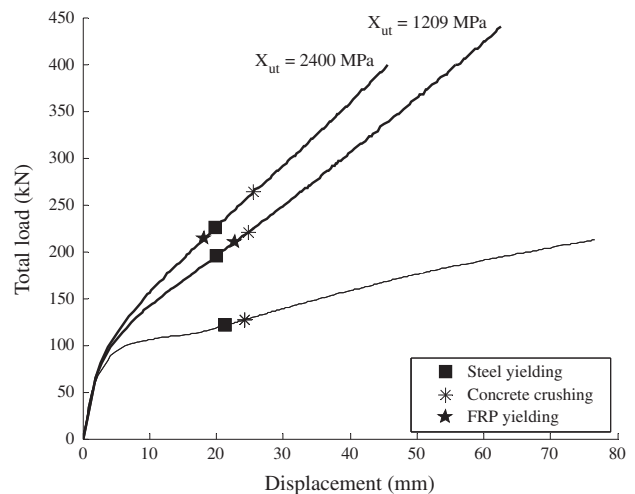
Adding more layers of FRP will not significantly increase the capacity of the composite slabs. This situation is shown in Fig. 13, where the ultimate loads for 1 layer and 2 layers of FRP laminate are almost the same, 391 kN (1 layer FRP) and 440 kN (2 layers FRP), respectively, while the ultimate loads for 3 layers (401 kN) and 4 layers of FRP (375 kN) are less if compared to two layers of FRP laminate. Although more FRP layers indicate more reinforcement adhered onto RC slabs, results show that the strengthened slabs fail to reach the expected ultimate loads.

Fig. 14 demonstrates similar crack patterns at the failure points for one-layer, two-layer, three-layer, and four-layer FRP laminate. The slabs do not appear to have more cracks; however, the ultimate loads for more FRP layers are smaller. Similar patterns indicate that the concrete is not the failure factor in the models. Furthermore, the interfacial shear stress is plotted in Fig. 15 to demonstrate the behavior of the interface between concrete and FRP. As the distance becomes closer to the center of the slab, the interfacial shear stress becomes higher. The total load and the maximum interfacial shear stress are parallel. The greater the number of layers attached, the earlier the maximum interfacial shear stress is reached. The maximum interfacial shear stress at ultimate load is similar to the interface behavior analysis of Mossalam’s FRP-strengthened RC slab by Elsayed et al. [10]. Their results indicate that the failure of an interface tends to dominate when more FRP layers are attached.

Comparing the results of the FB and CB assumption in Fig. 16, the curves for the FB assumption are too stiff and overestimated, especially at higher numbers of FRP layers. As more layers are attached to the slabs, the ultimate loads become increasingly overestimated. For example, the results from the FB ultimate load are overestimated 1.5 times ( $n_{layer} = 3$ ) and 2.2 times ( $n_{layer} = 4$ ) if they are compared to the CB results. An effective bond length exists beyond which an extension of the bond length cannot increase the bond strength as well as the ultimate load of the strengthened RC structure. As long as the criterion for the effective bond length

has been fulfilled, it is quite justifiable to use the perfect bonding assumption.

For the next models, another case of FRP properties was considered, tensile strength  $X_{ut} = 2400$  MPa and elastic modulus ( $E_{11}$ ) = 155 GPa. A higher FRP tensile strength does not mean that a higher ultimate load can be obtained. This is illustrated in Fig. 17 where for almost double the FRP tensile strength, the curve is slightly stiffer but a smaller ultimate load can be resisted by the composite. This fact shows that the bond and the properties of FRP affect the composite slabs. The failure for the slab with  $X_{ut} = 1209$  - MPa is steel yielding followed by concrete crushing and intact FRP; while the failure for the slab with  $X_{ut} = 2400$  MPa is FRP yielding followed by steel yielding, concrete crushing and intact FRP. The



**Fig. 17.** Load and mid-span displacement behaviors of RC square slabs with and without FRP for variations of FRP strength.

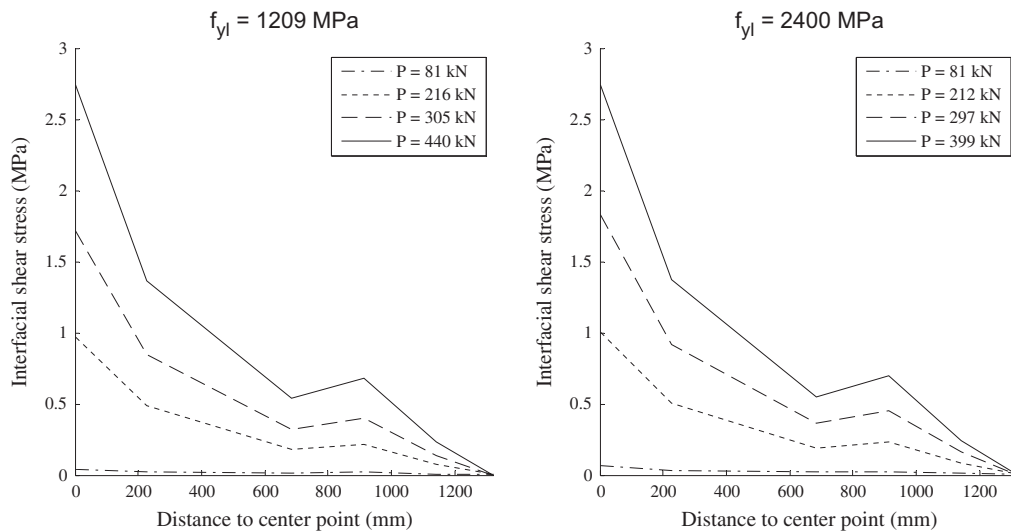


Fig. 18. Interfacial shear stress of FRP-strengthened RC slabs for different tensile strengths of FRP.

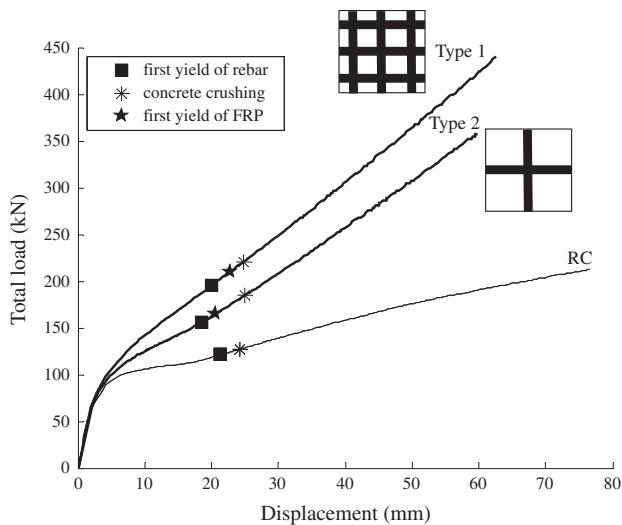


Fig. 19. Load and mid-span displacement behaviors of FRP-strengthened RC slabs for different strengthening schemes.

slabs adhered by carbon FRP are prone to fail by interface failure, not by the matrix failure or FRP failure. Consequently, the bond or interface is the most urgent factor to consider during numerical analysis.

Similar with Fig. 15, the results of the interfacial shear stress in Fig. 18 also demonstrate that the ultimate load is attained when the interfacial shear stress achieves its maximum value. Higher FRP tensile strength with small yielding strain specification leads the slab to reach the maximum interfacial shear stress faster. The interface failure is not only influenced by area of FRP, but also by the property of FRP. The higher the values of FRP area or property, the more FRP-strengthened slabs are prone to have interface failure.

A composite with bigger FRP area can achieve a higher ultimate load and stiffer curve. This is presented in Fig. 19, where adding more FRP strips is equivalent to adding more reinforcement into the slabs. They can increase the ultimate load of the composite until a certain limit. The failure modes for both models are similar: steel yielding followed by concrete crushing and intact FRP. However, the FRP yield is faster for the slabs with smaller FRP area (see Fig. 19).

## 5. Conclusions

In this paper, nonlinear FE analyses for strengthening square RC slabs by bonding FRP were performed. Based on the numerical results, the following conclusions may be drawn:

1. Tension stiffening is not sensitive to the ultimate load.
2. The FE results for the fully bonded assumption are too stiff compared to the results that include interface modeling.
3. An increased thickness of the slab can lead to a better composite design since the model can absorb more energy. However, as the thickness becomes less, the effects of FRP as a strengthening material are more significant.
4. The effects of the concrete strength properties are more significant for FRP-strengthened RC slabs compared to pure RC slabs. However, the modification of concrete strength properties only influence a small amount of the total energy stored at failure generally.
5. The increase of ultimate load for FRP-strengthened RC slabs compared with pure RC slabs is more significant when the slabs have lower steel reinforcement ratio. Using lower steel strength is recommended in order to utilize FRP, since FRP can make up for the shortcoming of steel.
6. Adding more layers of FRP will not significantly increase the capacity of the composite slabs. The maximum interfacial shear stress can be earlier reached when more FRP layers attached. Once the bond between RC and FRP is failed due to interfacial shear stress, adding more layers of FRP will be useless and will not increase the ultimate capacity of the structure. Therefore, a proper interface model should be incorporated into the numerical analysis.

## References

- [1] Fraldi M, Nunziante L, Carannante F, Prota A, Manfredi G, Cosenza E. On the prediction of the collapse load of circular concrete columns confined by FRP. *Eng Struct* 2008;30(11):3247–64.
- [2] Vougioukas E, Zeris CA, Kotsovos MD. Toward safe and efficient use of fiber-reinforced polymer for repair and strengthening of reinforced concrete structures. *ACI Struct J* 2005;102(4):525–34.
- [3] Teng J, Chen J, Smith S, Lam L. *FRP strengthened RC structures*. John Wiley & Sons Inc.; 2002.
- [4] Mosallam AS, Mosalam KM. Strengthening of two-way concrete slabs with FRP composite laminates. *Constr Build Mater* 2003;17(1):43–54.

- [5] Modena C. Fiber-reinforced polymer shear strengthening of reinforced concrete beams: experimental study and analytical modeling. *ACI Struct J* 2006;103(5):720–8.
- [6] Hu HT, Lin FM, Liu HT, Huang YF, Pan TC. Constitutive modeling of reinforced concrete and prestressed concrete structures strengthened by fiber-reinforced plastics. *Compos Struct* 2010;92(7):1640–50.
- [7] Hu H-T, Lin F-M, Jan Y-Y. Nonlinear finite element analysis of reinforced concrete beams strengthened by fiber-reinforced plastics. *Compos Struct* 2004;63(3–4):271–81.
- [8] Aprile A, Feo L. Concrete cover rip-off of R/C beams strengthened with FRP composites. *Compos Part B: Eng* 2007;38(5–6):759–71.
- [9] Chen GM, Chen JF, Teng JG. On the finite element modelling of RC beams shear-strengthened with FRP. *Constr Build Mater* 2012;32:13–26.
- [10] Elsayed W, Ebead UA, Neale KW. Interfacial behavior and debonding failures in FRP-strengthened concrete slabs. *J Compos Constr* 2007;11(6):619–28.
- [11] Mahini SS, Ronagh HR. Numerical modelling of FRP strengthened RC beam-column joints. *Struct Eng Mech* 2009;32(5):649–65.
- [12] Coronado CA, Lopez MM. Sensitivity analysis of reinforced concrete beams strengthened with FRP laminates. *Cem Concr Compos* 2006;28(1):102–14.
- [13] Neubauer U, Rostasy FS. Bond failure of concrete fiber reinforced polymer plates at inclined cracks—experiments and fracture mechanics model. In: 4th International symposium on fiber reinforced polymer reinforcement for reinforced concrete structures. Farmington Hills (MI): ACI; 1999. p. 369–82.
- [14] Nakaba K, Kanakubo T, Furuta T, Yoshizawa H. Bond behaviour between fiber-reinforced polymer laminates and concrete. *ACI Struct J* 2001;98(3):359–67.
- [15] Lu XZ, Teng JG, Ye LP, Jiang JJ. Bond–slip models for FRP sheets/plates bonded to concrete. *Eng Struct* 2005;27(6):920–37.
- [16] Hahn HT, Tsai SW. Nonlinear elastic behavior of unidirectional composite laminae. *J Compos Mater* 1973;7(1):102–18.
- [17] Jones RM, Morgan HS. Analysis of nonlinear stress–strain behavior of fiber-reinforced composite materials. *AIAA J* 1977;15(12):1669–76.
- [18] ACI-440. State-of-the-Art Report on Fiber Reinforced Plastic (FRP) Reinforcement for Concrete Structures (ACI 440R-96): American Concrete Institute; 2002.
- [19] Abaqus Inc. Abaqus Analysis User's Manuals and Example Problems Manuals. Version 6.10 Providence, Rhode Island; 2010.
- [20] Kupfer H, Hilsdorf HK, Rusch H. Behavior of concrete under biaxial stresses. *ACI Struct J* 1969;66(8):656–66.
- [21] Saenz L. Discussion of “Equation for the stress–strain curve of concrete” by Desayi P and Krishnan S. *ACI Struct J* 1964;61(9):1229–35.
- [22] Hu HT, Schnobrich WC. Constitutive modeling of concrete by using nonassociated plasticity. *J Mater Civil Eng ASCE* 1989;1(4):199–216.
- [23] ACI Committee 318. Building Code Requirements for Structural Concrete and Commentary (ACI 318-08). Detroit, Michigan; 2008.
- [24] ASCE Task Committee on Concrete and Masonry Structure. State of the art report on finite element analysis of reinforced concrete. ASCE; 1982.
- [25] Hu H-T, Schnobrich WC. Nonlinear analysis of cracked reinforced concrete. *ACI Struct J* 1990;87(2):199–207.
- [26] Mindlin RD. Influence of rotary inertia and shear on flexural motions of isotropic, elastic plates. *ASME J Appl Mech* 1951;18:31–8.
- [27] Tsai SW, Wu EM. A general theory of strength for anisotropic materials. *J Compos Mater* 1971;5(1):58–80.
- [28] Narayanaswami R, Adelman HM. Evaluation of the tensor polynomial and Hoffman strength theories for composite materials. *J Compos Mater* 1977;11(4):366–77.